Coded aperture imaging: the modulation transfer function for uniformly redundant arrays

E. E. Fenimore

Coded aperture imaging uses many pinholes to increase the SNR for intrinsically weak sources when the radiation can be neither reflected nor refracted. Effectively, the signal is multiplexed onto an image and then decoded, often by computer, to form a reconstructed image. We derive the modulation transfer function (MTF) of such a system employing uniformly redundant arrays (URA). We show that the MTF of a URA system is virtually the same as the MTF of an individual pinhole regardless of the shape or size of the pinhole. Thus, only the location of the pinholes is important for optimum multiplexing and decoding. The shape and size of the pinholes can then be selected based on other criteria. For example, one can generate self-supporting patterns, useful for energies typically encountered in the imaging of laser-driven compressions or in soft x-ray astronomy. Such patterns contain holes that are all the same size, easing the etching or plating fabrication efforts for the apertures. A new reconstruction method is introduced called δ decoding. It improves the resolution capabilities of a coded aperture system by mitigating a blur often introduced during the reconstruction step.

I. Introduction

For many situations in which an x-ray image is sought, one is faced with the problem that the x rays neither refract nor reflect. Thus, normal optics cannot be used. Two systems that can be used are the single-pinhole camera and the rastering collimator. Both systems usually require very long exposure times due to the inherently weak nature of many x-ray sources. Given the same resources of time and available detector area, both the pinhole and the rastering collimators produce images with approximately the same quality, that is, the same signal-to-noise ratio (SNR). Coded aperture imaging is a technique that seeks to overcome the normally poor SNR in x-ray imaging.

In coded aperture imaging, the pinhole of the simple pinhole camera is replaced by many pinholes arranged in some pattern. The recorded picture consists of many overlapping images of the x-ray source, one image from each pinhole. The overlapping is so severe that the recorded picture usually bears no resemblance to the x-ray object. This necessitates some form of processing of the recorded picture to reconstruct the x-ray object.

The author is with University of California, Los Alamos Scientific Laboratory, P.O. Box 1663, Los Alamos, New Mexico 87545.

Received 10 January 1980.
0003-6935/80/142465-07$00.50/0.

The usual goal of coded aperture imaging is to improve the image by increasing the collecting area with the use of many pinholes but maintain the same angular resolution as a single pinhole. To accomplish this goal, a suitable choice for the pinhole pattern and decoding method must be made. A simple mathematical model gives insight into how those choices should be made. If $A(x,y)$ is the aperture transmission and $S(x,y)$ is the x-ray object, the expected value of the recorded picture can be modeled as[1,3]

$$P(x,y) = S(x,y) * A(x,y) + N(x,y), \quad (1)$$

where $*$ is the correlation operator, and $N(x,y)$ is a signal-independent noise. Signal-independent noise is considered to be whatever signal is not modulated by the aperture (e.g., the signal due to cosmic rays, electronic noise). The usual method of decoding is by filtering the picture to reconstruct the x-ray source, that is, the reconstructed source can be found as

$$R(x,y) = P(x,y) * G(x,y) = S * [A * G] + N * G, \quad (2)$$

where $G(x,y)$ is referred to as the decoding function.

Equations (1) and (2) provide the basis for criteria for the selection of A and G. A and G should be chosen so that the reconstructed image is a faithful representation of the x-ray object at a resolution commensurate with a typical opening in the aperture. A and G should also not allow noise to dominate the reconstruction. The modulation transfer function (MTF) is useful in determining how faithful and how susceptible to noise the system is. The MTF indicates, as a function of spatial

frequency, how efficient the imaging system is in passing frequency information. If the MTF has a zero value at some frequency, the image after processing no longer contains any structure with that frequency. If the MTF has a low value, the image after processing does not contain that frequency at the same strength as in the original object. Rather, the amplitude of that frequency component is proportional to the MTF.

In principle, one wants a MTF that is monovalued so that all frequencies are passed equally well. In practice, the noise in the system and the finite size pinholes prevent monovalued MTFs. For example, from Eq. (2) $A * G$ is recognized as the system point-spread function (SPSF). As such, the frequency response of the system is

$$\mathrm{MTF}_{A*G} = |F(A * G)| = |F(A) \cdot F(G)|, \tag{3}$$

where F is the Fourier transform operator, and for simplicity we have not included the normalization to unity at zero frequency. By choosing G to be the correlational inverse, $A * G$ becomes a δ function, and the MTF is monovalued. However, for any actual aperture, $F(A)$ is not monovalued, typically falling off at high frequencies due to the finite size of the pinholes. Thus, for the MTF of the system to be monovalued, $F(G)$ must have large values so that $F(A) \cdot F(G)$ is constant. Although this in principle would provide an optimum SPSF, the large values in $F(G)$ could cause the noise term $(N * G)$ in Eq. (2) to dominate the reconstructed image.

We are faced with the following requirements for A and G:

(1) The SPSF should be similar to a δ function so that the reconstructed image is a faithful representation of the true object. In frequency space this means that the MTF of $A * G$ should be as flat as possible. Another way of stating this is to say that $A * G$ should pass all frequencies equally well, realizing that it undoubtedly falls off at high frequencies.

(2) To mitigate the effects of the noise, the MTF of A should be as flat as possible. If the MTF of A is monovalued, $F(G)$ will not require excessively large terms to produce a δ function SPSF [see Eq. (3)]. An alternate way of stating this requirement is that A should pass all frequencies equally well.

These requirements on A and G have not been met by most of the proposed aperture patterns. Fresnel zone plates,[1,2] particularly those with few zones (e.g., <50), and random arrays[3] have a range of values in their MTFs. The range of values means that the recorded picture will not have the same distribution of frequencies as the original object. If the reconstructed image does not have the same frequency distribution as the original object, the reconstructed image will not be a faithful image of the original object, an undesirable situation. One way for the system to produce a reconstruction that does have the same frequency distribution is to have the G function increase those frequencies that are low. This compensates for the fact that the aperture did not pass those frequencies as well as others. Such an analysis uses a G function related to the convolutional inverse of A. It requires G to enhance some frequencies in the recorded picture. Unfortunately, G also enhances whatever noise is present at those frequencies in the recorded picture. The enhanced noise often dominates the reconstruction. As an alternative, it is common to use for G either A or a scaled version of A.[2-5] Such an analysis (referred to as a correlation analysis or matched filtering) reduces the potentially damaging effects of the noise term. However, the SPSF is not a δ function, and artifacts are introduced into the reconstruction.[2,4,5] In either case (convolutional inverse or correlation analysis) the reconstructed object can differ from the original object.

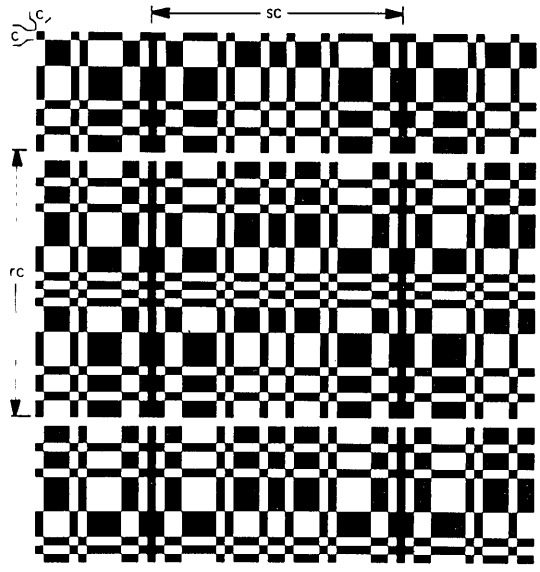

Fig. 1. Two cycles of an $r \times s$ URA pattern. Note it has periods rc and sc with square $c \times c$ pinholes.

Recently, a new type of pattern was proposed called uniformly redundant arrays[6] (URA), which can satisfy both the requirement for a δ function like SPSF and good noise handling characteristics. It is the purpose of this paper to derive the MTF for URA patterns. The insight gained from the derivation will be used to improve the design and decoding method of URA imaging systems.

II. MTF of the URA Aperture

Although there are several types of URA functions,[6] they all have the following three characteristics:

(1) They can be periodic, and in fact URAs are usually implemented as a mosaic of two cycles of a basic URA pattern.[6] Figure 1 is a typical URA mosaic. Each pinhole is a $c \times c$ area, and the basic pattern contains $r \times s$ elements. Thus, the mosaic has a period of rc in one direction and sc in the other.

(2) The centers of the holes can occur only at equally spaced grid points. In Fig. 1, the spacing is c.

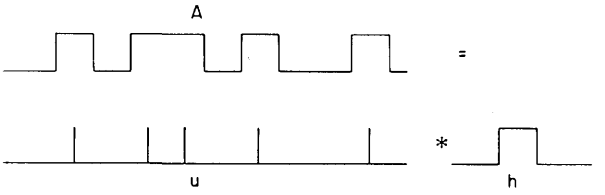

Fig. 2. Demonstration of how the aperture function can be decomposed into a function describing the locations of the pinholes and a function representing the pinhole shape.

(3) If the aperture is represented by a computer array (as in Ref. 6), the cyclic autocorrelation has a peak at zero lag (equal to d_0) and is monovalued (value d_1) at all other lags.

Figure 2 is a 1-D scan through a section of $A(x,y)$ and demonstrates how the aperture function can be represented as a convolution of a pinhole function $[h(x,y)]$, which describes the shape of the individual pinholes, and a function consisting of δ functions at those grid points which contain a hole $[u(x,y)]$. The complete description of $A(x,y)$ includes a box function $b(x,y)$, which limits the intrinsically infinite $u(x,y)$ function to some finite size. In practice, the aperture usually consists of two cycles of the URA function. However, in the reconstruction step an area of the recorded picture equal to only one cycle is used in a cyclic correlation. The MTF of such a system is characterized by a $b(x,y)$ function, which limits the aperture to one cycle. Therefore, we will use $b(x,y)$ equal to one only if $0 < x < rc$ and $0 < y < sc$ and $b(x,y)$ equal to zero otherwise.

Given these functions, the aperture can be represented as (Fig. 2)

$$A(x,y) = [u(x,y) * h(x,y)]b(x,y). \tag{4}$$

The properties of the Fourier transform of the aperture can be derived from Eq. (4) and the properties of $u(x,y)$. Equation (4) can be written in frequency space as

$$F(A) = [U(\mu,\nu) \cdot H(\mu,\nu)] * B(\mu,\nu). \tag{5}$$

Here, U, H, and B represent the Fourier transform of u, h, and b, respectively.

The first two of the above-mentioned characteristics of URAs give rise to properties of $U(\mu,\nu)$. Because u consists of δ functions that can occur only at spacing c, U is periodic with a period of $1/c$. In addition, since u is periodic (with a period of rc), U consists of δ functions at spacing $1/rc$, that is,

$$\begin{aligned} U(\mu,\nu) &= U(\mu + 1/c, \nu + 1/c), \\ U(\mu,\nu) &= \sum_{l=0}^{s-1}\sum_{k=0}^{r-1} D_{lk}\delta(\mu - k/rc)\delta(\nu - l/sc), \end{aligned} \tag{6}$$

when $0 < \mu < 1/c$ and $0 < \nu < 1/c$. Thus, U is completely determined by the rs values of D_{lk}. One portion of our task in determining the MTF of a URA pattern is to calculate all values of D_{lk}.

The correlation property of $A(x,y)$ [property (3) above] means that

$$\begin{aligned} u * u(x,y) &= u * u(x + rc, y + sc) \\ u * u(x,y) &= d_0\delta(x)\delta(y) + d_1 \sum_{l=1}^{s-1}\sum_{k=1}^{r-1} \delta(x - kc)\delta(y - lc), \end{aligned} \tag{7}$$

when $0 < x < rc$, $0 < y < sc$.

Since u is real and symmetric, $U^2 = F(u * u)$, and the Fourier transform of $u * u$ can give $|U|$. One can either apply the definition of a continuous Fourier transform to Eqs. (6) and (7) or one can use the relationships between discrete Fourier transform and continuous Fourier transform. Following the latter source, one recognizes [given Eq. (6) and the relationships in Ref. 7] that a discrete Fourier transform of $u * u(x,y)$ sampled on an $r \times s$ grid gives precisely $U^2(\mu,\nu)$ at frequencies k/rc and l/sc with $0 < k < r - 1$ and $0 < l < s - 1$. Because these are the only possible frequencies at which $|U(\mu,\nu)|$ has nonzero values [see Eq. (6)], the discrete Fourier transform can completely determine the continuous function $U^2(\mu,\nu)$. Equation (7) can be rewritten as

$$\begin{aligned} u * u(x,y) &= (d_0 - d_1)\delta(x)\delta(y) \\ &\quad + d_1 \sum_{l=0}^{s-1}\sum_{k=0}^{r-1} \delta(x - kc)\delta(y - lc), \end{aligned} \tag{8}$$

when $0 < x < rc$, $0 < y < sc$.

The discrete Fourier transform gives

$$\begin{aligned} U^2(\mu,\nu) &\propto d_1\delta(\mu)\delta(\nu) + [(d_0 - d_1)/rs] \\ &\quad \times \sum_{l=0}^{s-1}\sum_{k=0}^{r-1} \delta(\mu - k/rc)\delta(\nu - l/sc), \end{aligned} \tag{9}$$

when $0 < \mu < 1/c$ and $0 < \nu < 1/c$, where the standard constant of proportionality cannot be specified because technically the Fourier integral is infinite due to the infinite nature of $u(x,y)$.

Figure 3(a) shows a 1-D slice through a typical $|U(\mu,\nu)|$. $U(\mu,\nu)$ tells us how the multiplexing affects the frequency distribution in the recorded picture. (The effect of the hole shape will be considered below.) Fortunately, $|U(\mu,\nu)|$ is monovalued except at $(I/c, J/c)$, where I and J are integers. Thus, all frequencies are passed equally well except $(I/c, J/c)$, which are passed very strongly. The URA can be considered a phase-scrambling encoding system, which forms a recorded image with the same frequency information as in the original object.

Since Eq. (9) gives only U^2, we have not determined the complex phase of $U(\mu,\nu)$. The phase can be found by applying the definition of a discrete Fourier transform directly to $u(x,y)$. For example, for the URAs of Ref. 6, we found that the phase assumes only four different values within $U(\mu,\nu)$. The terms $U(k/rc, 0)$ and $U(0, l/sc)$ are real with opposite signs. The remaining terms have phase $\pm\beta$, where β depends on the particular URA pattern. We have also found that

$$\begin{aligned} U(k/rc, l/sc) &= \beta \text{ if } A(kc,lc) = 1 \\ &= -\beta \text{ if } A(kc,lc) = 0, \end{aligned} \tag{10}$$

where $k \neq 0$, and $l \neq 0$. Thus, the phases in $U(\mu,\nu)$ have the same pattern as the pattern of pinholes and solid material in the aperture. Note that, given Eqs. (8)–(10), one can completely determine $U(\mu,\nu)$ by calculating one $U(k/rc, l/sc)$.

The complete determination of $F(A)$ involves $U(\mu,\nu)$, $H(\mu,\nu)$, and $B(\mu,\nu)$. For example, if each hole consists of a $c \times c$ area (as in Fig. 1),

$$H(\mu,\nu) \propto \sin(2\pi c\mu)\sin(2\pi c\nu)/\mu\nu. \quad (11)$$

Figure 3(b) plots $H(\mu,\nu)$, and Fig. 3(c) shows $|U(\mu,\nu) \times H(\mu,\nu)|$. The infinite and periodic nature of $u(x,y)$ gives rise to the discrete nature of Fig. 3(c). In practice, $A(x,y)$ is usually limited in extent resulting in a continuous function for $F(A)$ [see Eq. (5)]. Using the $b(x,y)$, which limits $A(x,y)$ to one cycle, gives

$$B(\mu,\nu) \propto \sin(\pi cr\mu)\sin(\pi cs\nu)/\mu\nu, \quad (12)$$

which is plotted in Fig. 3(d). Figure 3(e) shows a typical URA MTF, that is, $|F(A)|$ [calculated by Eq. (5)].

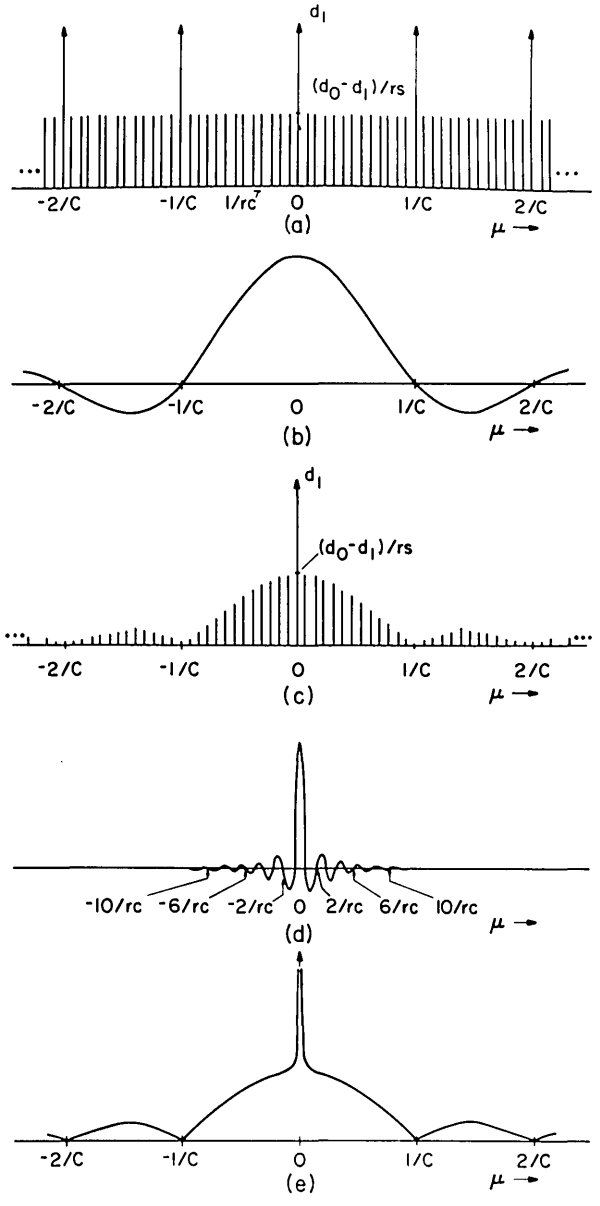

Fig. 3. Various functions used to derive the MTF of a URA aperture: (a) $|U(\mu,\nu)|$; (b) $H(\mu,\nu)$; (c) $|U(\mu,\nu) \cdot H(\mu,\nu)|$; (d) $B(\mu,\nu)$; (e) $|F(A)|$.

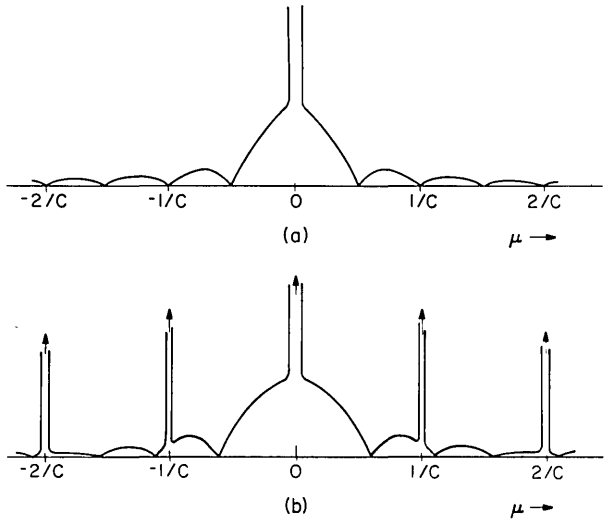

Fig. 4. (a) MTF of a URA whose pinholes are $c/2 \times c/2$ squares; (b) MTF of a URA whose pinholes are round with a diameter of $c/2$.

Note that the practical effect of $B(\mu,\nu)$ is to blur together the δ functions of $U(\mu,\nu)H(\mu,\nu)$. This gives rise to the primary result of this paper, which is that $F(A)$ is very well approximated as $H(\mu,\nu)$. The only practical differences are at the dc term and perhaps at values of (μ,ν) equal to $(I/c, J/c)$. Thus, the MTF of a URA pattern is virtually the same as the MTF of a single individual pinhole in the pattern.

The complex convolution of $(U \cdot H)$ with B might not be expected to be as well behaved as the absolute value of $F(A)$ because U has phase changes that might force $F(A)$ to have zeros. In fact, it is well behaved. The locations of the zeros in $B(\mu,\nu)$ are such that $F(A)$ is identically $H(\mu,\nu)$ at frequencies $(k/rc, l/sc)$ if the picture array has one sample per $c \times c$ area. When more samples per $c \times c$ area are taken (i.e., fine sampling), the phase does not change in a manner that could have $F(A)$ very different from $H(\mu,\nu)$ at any frequency sampled (except perhaps $I/c, J/c$). (This assumes that there is an integer number of samples per $c \times c$ area.) Thus, in a digital implementation of the decoding, the frequencies sampled always have the value $H(\mu,\nu)$ except at I/c, J/c. In summary, the decoding cancels whatever phase scrambling there is.

Figure 4 gives two examples of the MTF of some aperture functions. For Fig. 4(a) it was assumed that each hole was a $c/2 \times c/2$ square (with c being the separation between adjacent holes). Note that the peaks in $U(\mu,\nu)$ at $(I/c, J/c)$ do not affect $F(A)$ because they always occur at a zero in $H(\mu,\nu)$. For Fig. 4(b) it was assumed that each hole was round with a diameter of $c/2$. This results in an Airy disk for $H(\mu,\nu)$ and $F(A)$ that contains spikes at $(I/c, J/c)$.

It is instructive to compare the MTF of a URA pattern with the MTF expected for another commonly used coded aperture, the random array.[3] Of course, an infinite random array has the same properties as a URA. The following comments refer only to finite random arrays. The random array can be decomposed into a

$u_R(x,y)$ and $h_R(x,y)$, and the corresponding $U_R(\mu,\nu)$ can be calculated. Here the subscript R refers to random. Figure 5(a) is a 1-D slice through $U_R(\mu,\nu)$ and is analogous to Fig. 3(a). Those frequencies at which $U_R(\mu,\nu)$ is small were not passed well by the aperture, and, thus, the recorded picture is not only phase scrambled but also amplitude scrambled.

Although $H_R(\mu,\nu)$ would be the same for both URAs and random arrays, the MTFs are different. Figure 4(b) is analogous to Fig. 3(e) and shows the MTF of a random array (assumed to be periodic for the sake of this demonstration). Although the overall trend of Fig. 4(b) is similar to Fig. 3(e), the random array MTF contains a range of values including very small terms due to the amplitude scrambling. In fact, we found[6] that roughly 15% of 32×32 random arrays have a zero in their transform at frequencies $<1/c$. For G to restore the amplitude at those frequencies where the MTF is small, G must at the same time enhance whatever noise is present at these frequencies. To avoid that enhanced noise, a G that restores the amplitudes is typically not used. Rather a correlation analysis is used, but that leads to artifacts. In contrast, the MTF of the URA is well behaved, falling off almost exactly as does the MTF of a single pinhole. The contribution by the noise to a URA reconstructed image has the same distribution (in frequency space) as would be expected by a single pinhole.

The comparison between the random array and the URA demonstrates that the good multiplexing properties of the URA are the result of the locations of the holes in the URA pattern and not their shape. Any hole shape can be used.

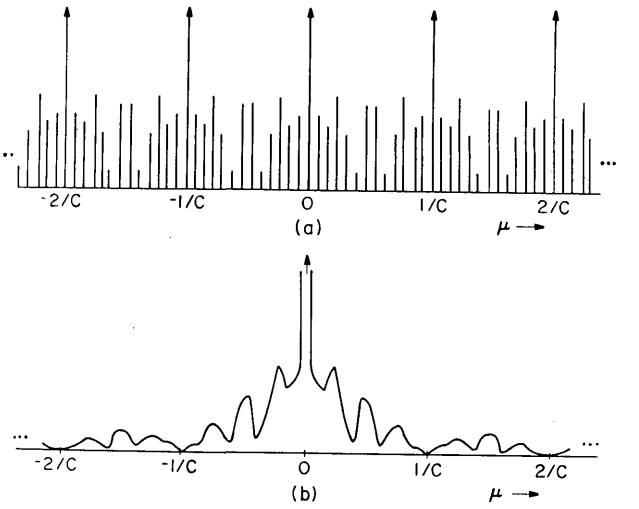

Fig. 5. (a) Fourier transform of $u(x,y)$ for a random array; (b) MTF of a random array.

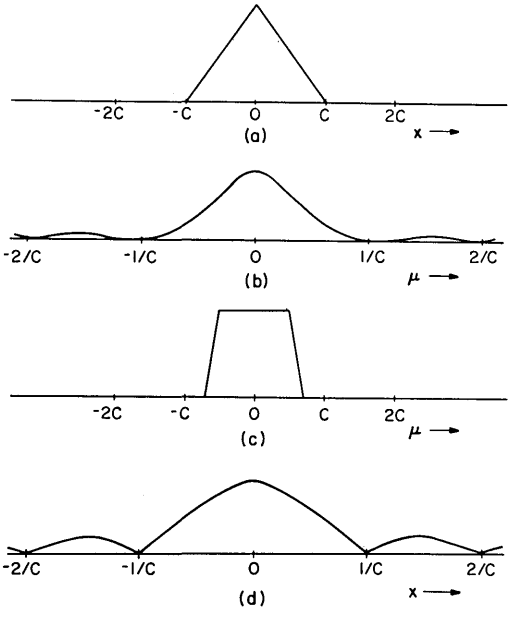

Fig. 6. (a) SPSF for a correlation analysis; (b) MTF for balanced correlation; (c) SPSF for δ decoding; (d) MTF for δ decoding.

III. Selection of the *A* and *G* Functions

The MTF of A derived in the previous section provides insight into the URA function, which can lead to improved capabilities. For example, it is the location of the holes (but not their shape) that produces the desirable characteristics of the MTF of the URA. By desirable we mean no small terms in $F(A)$, which would cause the noise term to dominate. Rather than being restricted to square holes of size $c \times c$, one can select a more convenient hole shape. Round holes offer the advantage of being easier (than square holes) to fabricate by various plating processes. In addition, by making the holes smaller than $c \times c$ the aperture becomes self-supporting with all holes the same size. Identical holes ease the fabrication effort. Note that the holes in Fig. 1 cause the aperture plate to fall apart. A supporting substrate eliminates this problem, but in some applications the x rays are at such a low energy that a substrate causes unacceptable absorption. For this reason, the recent[8] imaging of a laser-driven compression with a URA camera involved square holes of size $c/2 \times c/2$, which was self-supporting.

We now turn to the G function. The first G function proposed[1-3] was to use G equal to A (i.e., an autocorrelation analysis). The SPSF becomes $A * A$, which, assuming square holes, is a pyramid on top of a dc term (i.e., it is the convolution of two pinholes). One pinhole is inherent in the imaging for it arises from the pinholes in the aperture. The second pinhole arises from the fact that the recorded picture is correlated with a G function equal to A, which is equivalent to convolving with another pinhole. The MTF of the system (that is, including the encoding and decoding) is just the square of the MTF of the aperture $F^2(A)$.

Reconstructed images from an autocorrelation analysis contain large dc terms. That dc term can be removed by using balanced correlation[6,9] for which

$$G_B(x,y) = 1 \text{ if } A(x,y) = 1$$
$$G_B(x,y) = M/(M-N) \text{ if } A(x,y) \neq 1 \qquad (13)$$

when $0 < x < 2rs$, $0 < y < 2sc$; $G_B(x,y) = 0$, otherwise N is the number of holes in an rsc^2 area of the URA, and

M is the value of the side lobe of $A * A$ [see Eq. (4) of Ref. 9]. The subscript B refers to balanced correlation. Such a formulation for G_B has the effect of removing the dc term in $A * A$. However, the shape of the central peak in the SPSF is still a pyramid [Fig. 6(a)]. The resulting MTF is thus virtually the same as that obtained from two convolved pinholes [Fig. 6(b)].

The resolution of two convolved pinholes is inferior to that of a single pinhole [compare Fig. 6(b) with 3(e)]. It is inferior because the second of the two convolved pinholes adds an additional blur to the image. It is as if one forms a picture with a single pinhole [causing a blur whose MTF is shown in Fig. 3(b)] and then views that image through a second pinhole (causing the additional blurring). The origin of the second pinhole is the correlation of the recorded image with a G function containing finite sized pinhole areas.

The development of the URA MTF forms the basis for a new way to analyze coded aperture images, which mitigates this second blurring. In principle, the technique is to use

$$G_\delta(x,y) = u'(x,y) \cdot b(x,y), \tag{14}$$

where

$$u'(x,y) = 1 \text{ if } u(x,y) = 1$$
$$= M/(M-N)\delta(x - kc)\delta(y - lc) \text{ otherwise}$$

with $0 < k < 2r$, $0 < l < 2s$. The G_δ function is similar to G_B except it does not contain the hole shape function $h(x,y)$. Rather, it contains, in principle, δ functions (thus the name δ decoding). Note that G_δ does not have that component of $G_B(x,y)$, which contributes a second blurring during the reconstruction.

It is not possible to represent a infinitesimally thin δ function in the digital reconstruction, nor is it advisable, for the bandpass of a true δ function is infinite, probably causing a decreased SNR. In the digital implementation, the so-called δ functions are represented as a single element of a computer array, giving them an effective width. Typically, one might sample the recorded image in such a manner that the width of a single element represents about one-fourth of the width of the pinholes. Such δ decoding was used in the recent URA imaging of a laser-driven compression.[8]

Figure 6(c) is the SPSF for δ decoding. Note that it is virtually the same as a single pinhole response (i.e., a box function) except it is actually a trapezoid. The trapezoid results from the fact that the δ functions have some finite width associated with them. Employing arguments similar to those used to develop Eq. (9), one can show that

$$U'^2(\mu,\nu) \equiv F(u' * u') \propto \sum\sum \delta(\mu - k/rc)\delta(\nu - l/sc), \tag{15}$$

which is just equally spaced monovalued δ functions. The system MTF then becomes

$$\text{MTF}_s = |F(A * G_\delta)|$$
$$= |[U(\mu,\nu) \cdot H(\mu,\nu) * B(\mu,\nu)] \cdot [U'(\mu,\nu) \cdot H_\delta(\mu,\nu) * B(\mu,\nu)]|, \tag{16}$$

which is plotted in Fig. 6(d). $H_{\delta(\mu,\nu)}$ is the Fourier transform of a box function whose width equals the width represented by a single sample in the decoding array. Note that δ decoding has a better frequency response than that of a correlation analysis [i.e., Fig. 3(e)]. Delta decoding for optical reconstructions means using a mask in the reconstruction step that has smaller holes that the mask used as the aperture. Details of implementing δ decoding for digital reconstructions will be presented in a forthcoming paper.

The effects of diffraction and detector response can be easily included to complete the system MTF. If the detector has a point-spread function of $Q(x,y)$ and if the diffraction can be characterized with a point-spread function $D(x,y)$,

$$\text{MTF}_{\text{system}} = |F(A * G_\delta * D * Q)|. \tag{17}$$

It should be possible to use Eqs. (17) and (18) with standard image enhancement techniques to remove some of the single pinhole blurring, detector response blurring, and/or some of the diffraction.

IV. Summary

The URA avoids the near singularities inherent in the MTFs of other coded apertures. The study of the MTF of the URA aperture can provide insight into the workings of the URA, which can be used to improve its capabilities. We have derived the MTF by decomposing the URA into a function consisting of δ functions that describe the locations of the holes and a function that gives the shape of the individual holes. In frequency space, the function giving the locations has a flat Fourier transform except at $(I/c, J/c)$, where I and J are integers. The phase of $U(\mu,\nu)$ has a pattern that is the same as $A(x,y)$. The resulting MTF of the URA is virtually that of a simple individual hole. Thus, it is the location of the holes (independent of their shape) that provides the good imaging characteristics of the URA.

One is free to choose the shape of the individual holes. By making the holes smaller than the spacing between holes, the pattern becomes self-supporting, eliminating the need for a supporting substrate. This is an important advantage in the imaging of laser-driven compressions, which typically emit x rays that would be partially absorbed by a substrate. Since no two holes touch, all the holes can be the same size, greatly easing the fabrication effort if done by etching or plating. Round holes could also be used.

A new decoding method, called δ decoding, has been developed. Delta decoding mitigates a blurring that was present in previous correlation reconstruction procedures. The MTF of the system using δ decoding is virtually identical to that which would be obtained from a single pinhole of comparable size.

The author wishes to thank T. M. Cannon and H. J. Trussell for many helpful discussions and useful comments on the manuscript. This work was done under the auspices of the U.S. Department of Energy.

References

1. L. Mertz and N. Young, in *Proceedings, International Conference on Optical Instruments and Techniques*, K. J. Habell, Ed. (Chapman and Hall, London, 1961), p. 305.
2. H. H. Barrett and F. A. Horrigan, Appl. Opt. **12**, 2686 (1973).
3. R. H. Dicke, Astrophys. J. **153**, L101 (1968).
4. C. M. Brown, "Multiplex Imaging and Random Arrays," Ph.D. Thesis, U. Chicago (1972).
5. R. G. Simpson and H. H. Barrett, Opt. Eng. **14**, 490 (1975).
6. E. E. Fenimore and T. M. Cannon, Appl. Opt. **17**, 337 (1978).
7. E. O. Brigham, *The Fast Fourier Transform* (Prentice-Hall, Englewood Cliffs, N.J., 1974).
8. E. E. Fenimore, T. M. Cannon, D. B. Van Hulsteyn, and P. Lee, Appl. Opt. **18**, 945 (1979).
9. E. E. Fenimore, Appl. Opt. **17**, 3562 (1978).

Meetings Schedule

OPTICAL SOCIETY OF AMERICA
1816 Jefferson Place N.W.
Washington, D.C. 20036

15–17 July 1980 COHERENT LASER RADAR FOR ATMOSPHERIC SENSING, Aspen, Colo. Information: J. Connor at OSA or CIRCLE NO. 59 ON READER SERVICE CARD

28 July–8 August 1980 FIRST INTERNATIONAL WORKSHOP ON LIGHT ABSORPTION BY AEROSOL PARTICLES, Colorado State U., Fort Collins Information: Hermann E. Gerber, Physics Branch, Naval Research Laboratory, Washington, D.C. 20375

4–8 August 1980 OPTICS IN FOUR DIMENSIONS, Ensenada, Mexico Information: L. M. Narduzzi, Drexel U., Physics Dept., Philadelphia, Pa. 19104

16–18 September 1980 SIXTH EUROPEAN CONFERENCE ON OPTICAL COMMUNICATION, U. York Information: Secretariat, Conference Department, Institution of Electrical Engineers, Savoy Place, London WC2R, OBL, U.K.

22–23 September 1980 WORKSHOP ON OPTICAL FABRICATION AND TESTING, Boston Information: J. Connor at OSA or CIRCLE NO. 55 ON READER SERVICE CARD

6–9 October 1980 TENTH INTERNATIONAL LASER RADAR CONFERENCE, Silver Spring, Md. Information: Conference Secretariat: Tenth ILRC, c/o IPST, U. Maryland, College Park, Md. 20742

13–17 October 1980 ANNUAL MEETING OPTICAL SOCIETY OF AMERICA, Chicago Information: J. W. Quinn at OSA or CIRCLE NO. 61 ON READER SERVICE CARD

10–12 November 1980 SPECTROSCOPY IN SUPPORT OF ATMOSPHERIC MEASUREMENTS TOPICAL MEETING, Sarasota, Fla. Information: J. Connor at OSA or CIRCLE NO. 51 ON READER SERVICE CARD

1–3 December 1980 INFRARED LASERS TOPICAL MEETING, Lubbock, Tx. Information: J. Connor at OSA or CIRCLE NO. 60 ON READER SERVICE CARD

27–29 April 1981 THIRD INTERNATIONAL CONFERENCE ON INTEGRATED OPTICS AND OPTICAL FIBER COMMUNICATION, San Francisco Information: J. W. Quinn at OSA or CIRCLE NO. 56 ON READER SERVICE CARD

10–12 June 1981 CONFERENCE ON LASERS AND ELECTROOPTICS, Washington, D.C. Information: J. Connor at OSA or CIRCLE NO. 63 ON READER SERVICE CARD

8–11 September 1981 SEVENTH EUROPEAN CONFERENCE ON OPTICAL COMMUNICATION, Copenhagen Information: Magnus Danielsen, Conference Secretary, Technical University of Denmark, Electromagnetics Institute, Building 348, DK-2800 Lyngby, Denmark

26–30 October 1981 ANNUAL MEETING OPTICAL SOCIETY OF AMERICA, Kissimmee, Fla. Information: J. W. Quinn at OSA or CIRCLE NO. 57 ON READER SERVICE CARD

14–16 April 1982 CONFERENCE ON LASERS AND ELECTROOPTICS Phoenix Civic Plaza Convention Center Information: J. Connor at OSA or CIRCLE NO. 64 ON READER SERVICE CARD

18–22 October 1982 ANNUAL MEETING OPTICAL SOCIETY OF AMERICA, Tucson, Ariz. Information: J. W. Quinn at OSA or CIRCLE NO. 58 ON READER SERVICE CARD